Photochemical & Photobiological Sciences

PAPER

Cite this: *Photochem. Photobiol. Sci.*, 2015, **14**, 1941

The diffuse component of erythemal ultraviolet radiation

Abel A. Silva

The diffuse (Dif) component of ultraviolet radiation (UVR) plays an important role in the daily exposure of humans to solar radiation. This study proposes a semi-empirical method to obtain the Dif component of the erythemal dose rate, or the erythemally weighted irradiance, (EDR_{Dif}) calculated from synchronized measurements of the Dif component of UVR (UV_{Dif}) and the global (G) irradiances of both UVR (UV_G) and the erythemal dose rate (EDR_G). Since the study was conducted in the tropics, results involve a wide range of solar zenith angles to which EDR_{Dif} is seasonally dependent. Clouds are the main atmospheric agent affecting Dif radiation. The ratio between Dif and G (Dif/G) showed a quadratic dependence on cloud cover with a coefficient of determination $r^2 = 0.79$. The maxima of EDR_{Dif} were mainly above the moderate range (>137.5 mW m^{-2}) of the UV-Index and reached the extreme range (>262.5 mW m^{-2}) for the spring–summer period. The fraction of the global daily erythemal dose (daily ED_G) corresponding to Dif radiation (daily ED_{Dif}) ranged from 936 J m^{-2} to 5053 J m^{-2} and averaged 2673 J m^{-2}. Daily ED_{Dif} corresponded to at least 48% of daily ED_G for a practically cloudless sky. Therefore, Dif radiation is a real threat. Lighter skin people (types I and II) can get sunburnt in a couple of minutes under such an incidence of radiation. Moreover, accumulative harm can affect all skin types.

Received 30th March 2015,
Accepted 5th August 2015

DOI: 10.1039/c5pp00131e

www.rsc.org/pps

Introduction

Erythema (or sunburn) is a physiological reaction of the human skin against excessive exposure to ionizing and non-ionizing radiation.[1] In this case, the latter is represented by ultraviolet radiation (UVR; see Annex A for acronyms). A tan is another physiological reaction aiming to protect the skin from UVR to prevent erythema. Typically, a developed tan corresponds to a Solar Protection Factor of 3.[2,3] However, the complete development of a tan takes some hours after the exposure to UVR, and, in fact, that development depends crucially on the skin type. According to the skin classification by Fitzpatrick,[4] skin type I people (white-fair skinned, melano-compromised) will always get sunburnt and never get tanned if exposed for just a couple of minutes to UVR in the ranges of very high and extreme UV-Index (UVI).[5] It happens simply because the light skin cannot produce enough melanin to form a protective tan. On the other hand, skin type VI people (deep-black skinned, melano-protected) neither get burnt nor tanned. Nonetheless, all skin types (from I to VI) can be harmed by cumulative doses of UVR through biological effects like eye damage, immune suppression, DNA damage, photoaging, skin cancer, *etc.*[1] Note that the same melanin that protects from sunburn contributes to long term harm.[6,7]

However, the exposure to UVR in the range of 280–320 nm (or 280–315 nm in adherence to the Commission internationale de l'Éclairage, CIE)[1,5] (the UVB) brings not only harm, but also benefits through the induction of vitamin D (VD) synthesis in the human body.[1] VD is a hormone responsible for fixing calcium into the bones. For more than a century, low levels of VD (<75 nmol l^{-1} for insufficiency and <25 nmol l^{-1} for deficiency) in the serum have been associated with rickets, osteomalacia, and osteoporosis.[8–10] Although the VD needed by humans can be partially supplied by an appropriate diet, around 90% of that need comes from the exposure to the solar radiation.[11–13] Studies have shown that a few minutes in the noon Sun of a cloudless day with arms and hands free of sunscreen 3–4 times a week can provide people of skin types I and II with adequate serum concentrations of VD.[14–16] In addition, evidence linking VD and prevention of many diseases like some types of cancer (colon, prostate, and breast), diabetes I, multiple sclerosis, arthritis, *etc.* has mounted over the last few decades.[9,10,17,18]

Therefore, the exposure to UVR must be optimized. Since the Sun is the best and easiest source of UVR in the terrestrial biosphere, a conscious-selective concept of exposing the body partially to it should become a part of our regular photoprotection attitudes.[16,19–24] The conscious-selective concept proposes the reduction in the direct exposure to the Sun to avoid harm,

Instituto de Estudos Avançados, Rod. dos Tamoios km 5.5, Torrão de Ouro II, São José dos Campos, SP CEP 12228-001, Brazil. E-mail: abel@ieav.cta.br

but keeping some exposure at pre-determined daily periods to grasp at benefits. The appropriate UVR dose to avoid harm and grasp at benefits depends on the incidence of UVR as well as the behavior and physiology of individuals. The incidence of UVR can be analytically depicted by

$$G = \mathrm{Dif} + \mathrm{Dir}\cos(\mathrm{SZA}), \quad (1)$$

where G represents the global incidence of radiation on a flat horizontal surface (irradiance), while Dif and Dir are the diffuse and direct components, respectively, of G for a given solar zenith angle (SZA). Although the shade of a building, a hat, or an umbrella can shelter us from the Dir component of solar UVR, the Dif one represents a challenge in terms of being avoided.[25] Dif radiation results from the atmospheric scattering and surface reflection of solar radiation, being present even in the apparent safe interior of a building. However, the amount of data or quantitative information referring to that component in terms of biological effects like sunburn (or any other one) is scarce.

Despite the wide and indiscriminate advertisement by the pharmaceutical industry announcing the use of sunscreen as the ultimate solution to avoid harm from the exposure to solar radiation,[26] a growing number of skin cancer cases and other detrimental effects from being excessively in the Sun (with or without sunscreen) have been foreseen for the coming years.[1,5] In fact, the correct use of sunscreen does not completely avoid the absorption of UVR by the skin, and some residual amount of radiation will accumulate in the body with time, leading to detriments. Only recently the pharmaceutical industry has introduced, in the sunscreen formula, an absorber specific for radiation in the range of 320–380 nm (the UVA), which had been neglected for a long time due to the lack of knowledge (or doubt) regarding its deleterious effects.[7,27] The introduction of a conscious-selective concept for exposure as a common photoprotection method among people added to the use of sunscreen for UVB + UVA could perhaps represent an effective and more appropriate way to deal with the problem of overexposure.

Nevertheless, the avoidance of direct exposure to the Sun does not mean to be safe from solar radiation, since Dif radiation is always present in general.[25] In addition, studies on climate change have foreseen different levels of change across the world in both cloud cover and cloud type.[28] Such changes will probably lead to modification in the incidence of Dif radiation.

In this work, a semi-empirical method is presented to obtain the Dif component of the erythemal dose rate, or the erythemally weighted irradiance, ($\mathrm{EDR_{Dif}}$) of solar UVR on the basis of measurements of the global erythemal dose rate ($\mathrm{EDR_G}$) and the global and diffuse UVR rates ($\mathrm{UV_G}$ and $\mathrm{UV_{Dif}}$ respectively), considering the influence of cloud cover. Thus, site, equipment for measurements, and ancillary material are depicted in the Site, instruments and methods section, while the procedure to obtain $\mathrm{EDR_{Dif}}$ from $\mathrm{EDR_G}$, $\mathrm{UV_G}$, and $\mathrm{UV_{Dif}}$ is presented in the Methodology section. The main results and detailed information on $\mathrm{EDR_{Dif}}$ and its dependence on clouds are provided in the Results and discussion section. The main achievements are summarized in the Conclusions section. A list of acronyms is presented in Annex A.

Site, instruments and methods

Site description

Belo Horizonte (BH, 19.92°S, 43.94°W, 858 m a.s.l., 331 km^2, Brazil) is the center of the 3rd largest Brazilian metropolitan area with 5.4 million inhabitants. As a municipality, it has over 1.2 million vehicles featured with catalytic converter devices and electronic injection engines. Predominant economic activities in the region are trade and industry. Located in a hilly area of southeastern Brazil, the city features a tropical climate of altitude (milder weather due to site's altitude) between the savanna (Cerrado) and the remains of the Atlantic forest (Mata Atlântica). The dry period develops from May to September and the rainy one from November to March. Large amounts of biomass burning smoke are blown into the city during the former period. Seasons are split as: December, January, and February for summer; March, April, and May for fall; June, July, and August for winter; and September, October, and November for spring.

Biometer Solar Light

A Biometer Solar Light 501A (BSL, Solar Light Co., Inc., Glenside, USA) measures the UVR biologically weighted through an erythema action spectrum similar to the one by CIE,[29] which is shown in the middle frame of Fig. 1. Operating under a stabilized temperature of 25 °C, the instrument received daily maintenance by the operator and periodic calibration at the manufacturer facilities with reference sources for the evaluation of its spectral response. Measurements were cleared with quality control and quality assurance procedures and received

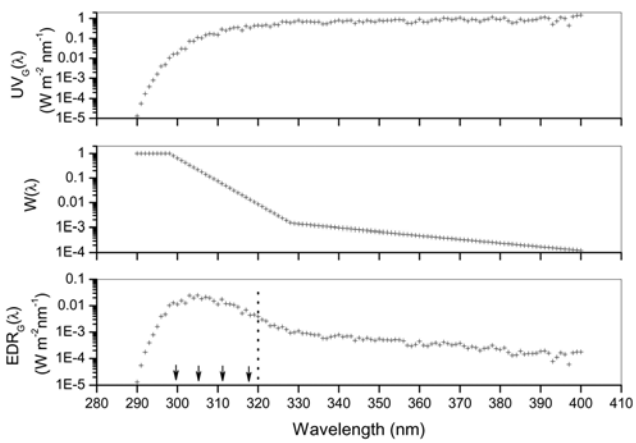

Fig. 1 (Top) $\mathrm{UV_G}(\lambda)$ in BH on JAN022010 at noon (15:00 UT) calculated by the FastRT model. (Middle) The erythema action spectrum $W(\lambda)$ proposed by CIE. (Bottom) The $\mathrm{EDR_G}(\lambda)$ corresponding to $\mathrm{UV_G}(\lambda)$ and also calculated using the FastRT model. The arrows indicate the four UVMFR4 wavelengths and the vertical dashed line marks the limit of 320 nm between UVB and UVA.

cosine response correction following a specific cosine response curve. Note that cosine correction is completely appropriated for the Dir component of radiation, but it is only partially appropriated for the Dif one. An overall uncertainty of at least 6.9% (1σ) is expected in the measurements.[30] These measurements are originally the erythemal dose (ED) within a time interval, and the ratio of ED to its corresponding time interval makes the average value of EDR_G.

Ultraviolet Rotating Shadowband Radiometer 4

The Ultraviolet Rotating Shadowband Radiometer 4 (UVMFR4, Yankee Environmental Systems, Inc., Turners Falls, USA) measures the spectral values of UV_G and UV_{Dif} at the nominal wavelengths of λ_1 = 300 nm, λ_2 = 305.3 nm, λ_3 = 311.5 nm, and λ_4 = 317.5 nm with a bandwidth of 2 nm. The Dir component of solar UVR (UV_{Dir}) is calculated through the application of eqn (1). The instrument uses a semi-circular metallic strip to obstruct the direct incidence of solar radiation in the instrument's sensor. For this, firstly, the strip is set in the home position by a stepper motor allowing the measurement of UV_G. Secondly, the strip is rotated to a central position blocking the sensor from UV_{Dir} and allowing the measurement of UV_{Dif}. However, part of the sky (≈3.3°) in addition to the solar disk is inevitably blocked. To compensate for the radiation lost from that part of the sky, another two measurements with the strip rotated 9° to the left and to the right off the central position are made. These measurements are called displaced-strip measurements. The difference between UV_G and the average between the displaced-strip measurements represents the amount of Dif radiation blocked out by the strip from the sky. That amount is added to the original measurement of UV_{Dif} as a correction. The cycle of four measurements (UV_G, UV_{Dif}, and the two displaced-strip measurements) takes 20 seconds. Therefore, the minute-rated measurements of UV_G, UV_{Dif}, and their corresponding UV_{Dir} are averages based on 3 cycles of measurements per minute. The UVMFR4 must be set up aligned with the meridional direction. Accuracy in the positioning of the semi-circular metallic strip is within 0.4°. The software controlling the instrument calculates both SZA and azimuth angle to set rightly the strip.

The instrument's sensor and its associate electronic circuit is housed and sealed against moisture and rain (the moisture seal of the stepper motor can fail within a few months). The instrument works with an internal temperature controlled around 41 °C–42 °C for outdoor temperatures from −30 °C to +50 °C. Cosine correction is automatic for UV_{Dir} with accuracy of 1% for SZA up to 80°, but no cosine correction is attempted for UV_{Dif}. Typical uncertainties in UV_G and UV_{Dif} are around 6%–8%.[31] Annual calibration with appropriate facilities is recommended to maintain such standards.

Total Sky Imager

A Total Sky Imager 440A (TSI, Yankee Environmental Systems, Inc., Turners Falls, USA) measures cloud cover (cloudiness). It is composed of a digital camera facing down a rotating spherical mirror to photograph the reflected sky. A black strip is attached to the mirror in order to avoid direct reflection of sunbeams into the camera. Each snapshot results in a 24-bit color Joint Photographic Experts Group (JPEG) image with resolution of 352 × 288 pixels. The software provided by the manufacturer and set up in a personal computer controls TSI and processes captured images to determine cloud cover. Some software's parameters must be adjusted by the operator in order to produce the best match between the cloud cover observed by a trained operator and that determined by the equipment. Uncertainties in cloud cover measurements are higher than 10%, in general.[32]

FastRT model

The radiation transfer model FastRT[33] (Fast and easy simulation tool ver. 2, http://nadir.nilu.no/~olaeng/fastrt/fastrt.html) is a routine computing downward irradiances on horizontal surfaces in the spectral range of 290–400 nm for several action spectra. Input parameters are site's coordinates, SZA, total ozone column (TOC), optical thicknesses of clouds and aerosols, cloud cover, and albedo. Irradiances are obtained by the interpolation of effective transmittances stored in look-up tables. These tables were computed using the multi-stream discrete ordinates radiative transfer equation solver (DISORT).

Methodology

The spectral UV_G can be converted into EDR_G if weighted by the erythema action spectrum $W(\lambda)$,[1,5]

$$EDR_G = \int_{\lambda_0}^{400} UV_G(\lambda) \cdot W(\lambda) \cdot d\lambda, \quad (2)$$

where the radiation wavelength λ has its inferior limit λ_0 > 250 nm depending on the site's altitude, SZA, TOC, and particle matter in the atmosphere. In general, λ_0 = 280 nm for altitudes around 800–900 m a.s.l. in the tropics of the southern hemisphere. A practical application of eqn (2) can be made for UV_G measurements on January 2 of 2010 (JAN022010) in BH. This was a clear-sky day with cloud cover below 3% and average TOC[34] of 257.8 ± 6.2 Dobson Units (DU) at noon (≈15:00 Universal Time, UT). Table 1 summarizes

Table 1 Parameters input into the FastRT model to determine the UV_G and EDR_G incidence in BH at the Laboratório de Luz Ultravioleta (LLUV) station's coordinates on JAN022010 at noon

Location	BH (LLUV)
Latitude	−19.92°S
Longitude	−43.99°W
Surface altitude (km)	0.91
Surface albedo	0.03 (dry concrete-asphalt)
Sky condition	Cloudless
Visibility (km)	25
Triangular spectral function	0.60 nm FWHM
Date	JAN022010
Day of year (DOY)	2
TOC (DU)[a]	257.8 ± 6.2 (1σ)

[a] DU stands for Dobson Units.

these values in addition to the parameters input into the FastRT model for the calculation of $UV_G(\lambda)$, which is depicted in the top frame of Fig. 1. The corresponding $EDR_G(\lambda)$ calculated by the FastRT model is shown in the bottom frame of Fig. 1. The application of eqn (2) makes EDR_G = 0.359 W m^{-2}, where 87% and 13% of this value are split between the ranges of UVB and UVA respectively. The value measured by BSL was 0.332 W m^{-2}. Thus, the difference between calculated and measured values is ≈8%, which is similar to the 1σ uncertainty in BSL's measurements.

The incidences of UV_G and EDR_G grow together, especially in the case of the former being solar UVR. It seems reasonable to investigate the hypothesis of EDR_G being linearly dependent on the sum (S_G) of the values of UV_G at the four UVMFR4 wavelengths (see the bottom frame of Fig. 1) for a given SZA. Thus,

$$\begin{aligned} EDR_G &= c + b[UV_G(\lambda_1) + UV_G(\lambda_2) + UV_G(\lambda_3) + UV_G(\lambda_4)] \\ &= c + b\cdot\sum_{i=1}^{4} UV_G(\lambda_i) \\ &= c + b\cdot S_G \end{aligned} \quad (3)$$

where b (nm) and c (W m^{-2}) are coefficients. The top frame of Fig. 2 depicts $UV_G(\lambda_i)$ values measured by UVMFR4 on JAN022010 and their sum S_G, while the bottom frame exhibits the corresponding measurements of $UV_{Dif}(\lambda_i)$ and their sum S_{Dif}.

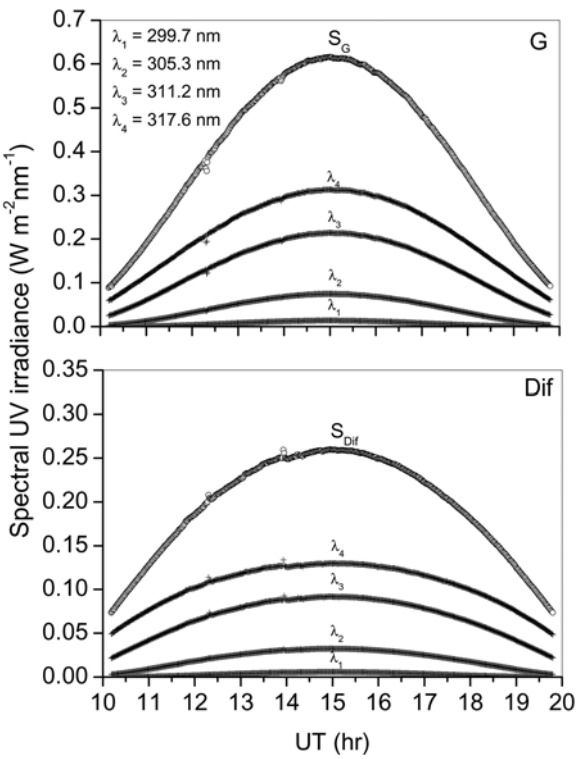

Fig. 2 (Top) Measurements of UV_G and (bottom) UV_{Dif} at the four UVMFR4 wavelengths on JAN022010 in BH. The corresponding sums of S_G and S_{Dif} are also shown.

The fraction of UV_G in the form of UV_{Dif} for a given λ_i is

$$f_{\lambda_i} = \frac{UV_{Dif}(\lambda_i)}{UV_G(\lambda_i)}. \quad (4)$$

The dependence of f_{λ_i} on λ_i within the range of the most significant UVR wavelengths for sunburn (≈UVB + part of UVA) is not strong, and the average value of f_{λ_i} ($\bar{f}_\lambda$) calculated within this range of wavelengths is associated with a small value of standard deviation, especially after weighting f_{λ_i} with the product $UV_{Dif}(\lambda)\cdot W(\lambda)$ to emphasize the contribution of UV_{Dif} sunburn wavelengths:

$$\bar{f}_\lambda = \frac{\int_{\lambda_0}^{400} \frac{UV_{Dif}(\lambda)}{UV_G(\lambda)} UV_{Dif}(\lambda)\cdot W(\lambda)\cdot d\lambda}{\int_{\lambda_0}^{400} UV_{Dif}(\lambda)\cdot W(\lambda)\cdot d\lambda}. \quad (5)$$

Arrows in the bottom frame of Fig. 1 indicate the four UVMFR4 wavelengths. They are regularly distributed among the most significant radiation wavelengths causing sunburn. Therefore, it is reasonable to affirm that

$$\bar{f}_\lambda \approx \bar{f}_4 = \frac{\sum_{i=1}^{4} \frac{UV_{Dif}(\lambda_i)}{UV_G(\lambda_i)} UV_{Dif}(\lambda_i)\cdot W(\lambda_i)\cdot \Delta\lambda_i}{\sum_{i=1}^{4} UV_{Dif}(\lambda_i)\cdot W(\lambda_i)\cdot \Delta\lambda_i}, \quad (6)$$

where $\Delta\lambda_i$ = 2 nm is the UVMFR4's wavelength bandwidth. The standard deviation of $\bar{f}_4$ can be calculated by

$$\sigma_{\bar{f}_4} = \sqrt{\frac{1}{3}\sum_{i=1}^{4} (f_{\lambda_i} - \bar{f}_4)^2}. \quad (7)$$

To check on the statements regarding $\bar{f}_4$, the right-sided frames of Fig. 3 show the average fraction $\bar{f}_4$ and its standard deviation for UVMFR4 measurements on the clear-sky and cloudless day of JAN022010 in addition to the partially cloudy and overcast days of October 16 (OCT162009) and December 9 (DEC092009) of 2009, respectively, in BH. In general, the association of $\bar{f}_4$ with small values of standard deviation is confirmed. Exception occurs for the larger values of SZA in early morning and late afternoon. The effect is caused by the increasing variability in the UVR scattering with the total atmospheric air mass, which depends not only on the larger radiation path through the free air, but also on the larger radiation path through clouds and aerosol parcels. On the other hand, the frame for JAN022010 depicts the already expected strong dependence of $\bar{f}_4$ on the SZA. Such dependence is hidden by the cloudy scenario on OCT162009 and DEC092009.

The linear regression analysis must be applied to a whole database of S_G *vs.* EDR_G with the same SZA to confirm the feasibility of eqn (3). Nonetheless, gathering such a set of data implies hundreds of days of measurements to guarantee a statistically significant analysis. Since the sky scenario can vary freely and largely among the days of measurements where clouds, aerosols and TOC make $\bar{f}_4$ vary deeply, the gathering of

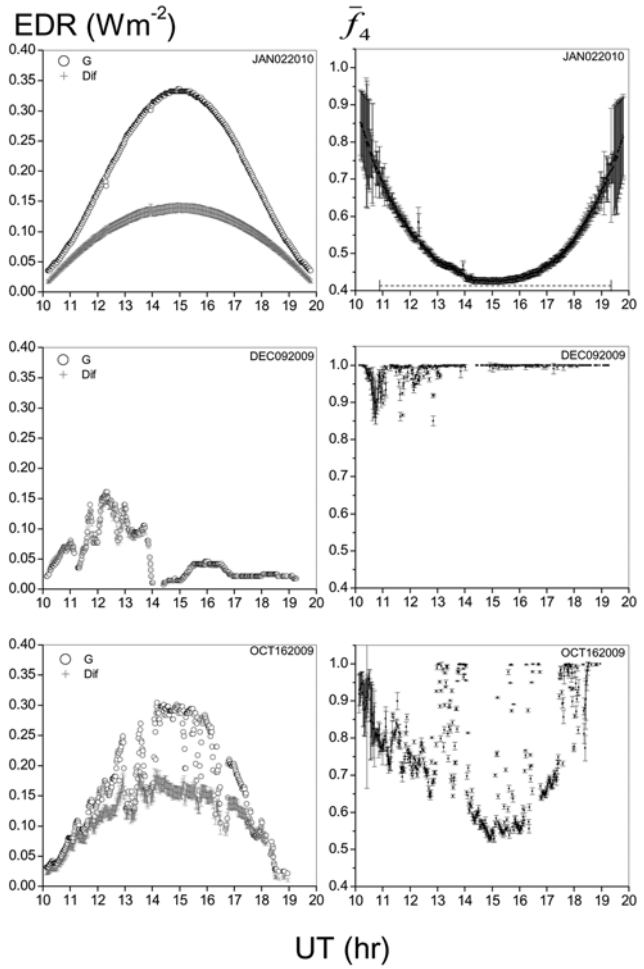

Fig. 3 (Left) EDR_G measurements and the calculated values of $EDR_{Dif} \pm 1\sigma$, and (right) the corresponding values of $\bar{f}_4 \pm 1\sigma$ for BH on (top) JAN022010, (middle) DEC092009, and (bottom) OCT162009. In the top-right frame, the dashed-horizontal line put just above the time axis indicates the period of time (corresponding to the percentage *T*%) regarding values of valid EDR_{Dif} on JAN022010.

a daily database with varying SZA would not represent a significant violation of the condition of a whole database with the same SZA, indeed. Therefore, instead of having only two pairs of values of S_G *vs.* EDR_G per day (one in the morning and the other in the afternoon), the use of databases of daily distributions of S_G *vs.* EDR_G would increase the number of pairs of data to the hundreds within the shorter period of a day. In fact, the variation in SZA and, consequently, $\bar{f}_4$ affects S_G and EDR_G similarly.

The application of the linear regression analysis to the database of S_G *vs.* EDR_G for a given day transforms eqn (3) into

$$EDR_G = c_d + b_d \cdot S_G, \quad (8)$$

where b_d and c_d are daily coefficients. This equation can be split into two parts following eqn (1):

$$EDR_{Dif} + EDR_{Dir}\cos(SZA) = c_d + b_d(S_{Dif} + S_{Dir}\cos(SZA)).$$

Since c_d can also be expressed as $c_d = c_{dDif} + c_{dDir}\cos(SZA)$,

$$EDR_{Dif} + EDR_{Dir}\cos(SZA) = c_{dDif} + c_{dDir}\cos(SZA) + b_d(S_{Dif} + S_{Dir}\cos(SZA)) \quad (9)$$

then

$$EDR_{Dif} = c_{dDif} + b_d \cdot S_{Dif}, \quad (9a)$$

$$EDR_{Dir}\cos(SZA) = c_{dDir}\cos(SZA) + b_d \cdot S_{Dir}\cos(SZA). \quad (9b)$$

As this study aims at the determination of Dif radiation, only eqn (9a) will be considered herein. Each pair of S_{Dif} *vs.* EDR_{Dif} corresponds to a value of $\bar{f}_\lambda$ (or $\bar{f}_4$). After eqn (4), it seems reasonable to affirm that $c_{dDif} = \bar{f}_\lambda \cdot c_d \approx \bar{f}_4 \cdot c_d$, making eqn (9a) as

$$EDR_{Dif} = \bar{f}_\lambda \cdot c_d + b_d \cdot S_{Dif} \approx \bar{f}_4 \cdot c_d + b_d \cdot S_{Dif}. \quad (10)$$

For independent and non-correlated variables on the right side of the equation, the application of the error propagation analysis yields the uncertainty in EDR_{Dif} as

$$\sigma_{EDR_{Dif}} \approx \sqrt{\bar{f}_4{}^2 \cdot \sigma_{c_d}{}^2 + c_d{}^2 \cdot \sigma_{\bar{f}_4}{}^2 + b_d{}^2 \cdot \sigma_{S_{Dif}}{}^2 + S_{Dif}{}^2 \cdot \sigma_{b_d}{}^2}, \quad (11)$$

where σ_{c_d}, $\sigma_{\bar{f}_4}$, $\sigma_{S_{Dif}}$, and σ_{b_d} represent the uncertainties in c_d, $\bar{f}_4$, S_{Dif}, and b_d respectively. σ_{c_d} and σ_{b_d} are drawn from the linear fitting of S_G *vs.* EDR_G reflecting the uncertainties in the measurements, $\sigma_{\bar{f}_4}$ is given by eqn (7), and

$$\sigma_{S_{Dif}} = 0.08 \cdot \sqrt{UV_{Dif}(\lambda_1)^2 + UV_{Dif}(\lambda_2)^2 + UV_{Dif}(\lambda_3)^2 + UV_{Dif}(\lambda_4)^2} \quad (12)$$

since $\sigma_{UV_{Dif}\lambda_1} \approx \sigma_{UV_{Dif}\lambda_2} \approx \sigma_{UV_{Dif}\lambda_3} \approx \sigma_{UV_{Dif}\lambda_4} \approx 8\%$ of the corresponding UV_{Dif} measurements by UVMFR4.

Thus, on the basis of measurements of EDR_G, UV_G, and UV_{Dif} the value of EDR_{Dif} and its uncertainty for a given SZA can be calculated through the use of eqn (10) and (11) respectively. A point to be considered here is that, the four UVMFR4 wavelengths are all in the UVB range. Although UVA makes a minor contribution to the typical highest values of EDR_G dominated by UVB, such a contribution can be significant as suggested by the bottom frame of Fig. 1. In fact, the relative contribution of UVA to EDR_G increases with both SZA and clouds blocking the Sun. Therefore, early morning, late afternoon, and cloudy skies represent situations of increasing relative contribution of UVA to EDR_G. Because of this, the linear relation of S_G *vs.* EDR_G becomes poorer at larger SZA and skies where Dir radiation is reduced by clouds.

The calculated value of EDR_{Dif} can be tested to identify such situations. For a strong linear relation between S_G and EDR_G, eqn (4) and (6) suggest that

$$EDR_{Dif} = \bar{f}_\lambda \cdot EDR_G \approx \bar{f}_4 \cdot EDR_G. \quad (13)$$

Then,

$$\rho = \frac{EDR_{Dif}}{\bar{f}_\lambda EDR_G} \approx \frac{EDR_{Dif}}{\bar{f}_4 EDR_G} \approx 1. \quad (14)$$

The application of the error propagation analysis to this equation makes

$$\sigma_\rho \approx \frac{1}{\bar{f}_4 \cdot \mathrm{EDR_G}} \sqrt{{\sigma_{\mathrm{EDR_{Dif}}}}^2 + \left(\frac{\sigma_{\mathrm{EDR_G}} \cdot \mathrm{EDR_{Dif}}}{\mathrm{EDR_G}}\right)^2 + \left(\frac{\sigma_{\bar{f}_4} \cdot \mathrm{EDR_{Dif}}}{\bar{f}_4}\right)^2}, \quad (15)$$

which features the uncertainty in taking a calculated value of $\mathrm{EDR_{Dif}}$ as correct. Only values of $\mathrm{EDR_{Dif}}$ to which

$$\rho \in [1 - \sigma_\rho, 1 + \sigma_\rho] \quad (16)$$

will be taken as correct (or valid $\mathrm{EDR_{Dif}}$), drawn from good quality linear fittings between S_G and $\mathrm{EDR_G}$. In the case of ρ being statistically represented by a normal distribution, the application of eqn (16) to the database implies that ≈68% of the $\mathrm{EDR_{Dif}}$ values would be valid $\mathrm{EDR_{Dif}}$.

The method described above was applied to the synchronized measurements made by the BSL #9007, the UVMFR4 #566 (operating with the specific wavelengths of λ_1 = 299.7 nm, λ_2 = 305.3 nm, λ_3 = 311.2 nm, and λ_4 = 317.6 nm), and the TSI #157 to obtain $\mathrm{EDR_{Dif}}$ and the daily erythemal dose of Dif radiation (daily $\mathrm{ED_{Dif}}$). The instruments were setup in the campus of the Pontifícia Universidade Católica de Minas Gerais (PUC Minas) in BH by the Laboratório de Luz Ultravioleta (LLUV, http://www.dfq.pucminas.br/PUV/index.html) in a platform to guarantee free-sky measurements from August 2009 to July 2010. Measurements were obtained at a rate of 1 measurement-per-minute. The temporal synchronization among the instruments occurred through the synchronization with an atomic clock *via* Internet, ensuring temporal uncertainties within 10 seconds. The values of cloud cover determined by TSI was hourly average values based on the concept of Local Cloud Cover over 60 minutes ($\mathrm{LCC_{60}}$) as described by Silva and Souza-Echer.[32]

Results and discussion

Measurements of $\mathrm{EDR_G}$, $\mathrm{UV_G}$, and $\mathrm{UV_{Dif}}$ were obtained for 293 days in the tropical, urban site of BH and analyzed to obtain $\mathrm{EDR_{Dif}}$ and $\mathrm{ED_{Dif}}$ on the basis of the potential linear relation between S_G and $\mathrm{EDR_G}$.

The linear relation between S_G and $\mathrm{EDR_G}$

It was hypothesized that a linear relation would be kept between S_G and $\mathrm{EDR_G}$. The application of the linear regression analysis to the database of S_G *vs.* $\mathrm{EDR_G}$ showed linear links of significant confidence level supporting that hypothesis. Such a statement is based on the values obtained for $b_d \pm \sigma_{b_d}$, $c_d \pm \sigma_{c_d}$, the coefficient of determination (r^2), and the percent scattering of points (SD%) around the fitting line. Fig. 4 shows b_d and c_d for the 293 days of measurements in this study. Most of the values are significant at 95% (2σ). Seasonal dependence of b_d has been identified with maximum values in summer. The explanation for this effect is the larger contribution of UVB to both S_G and $\mathrm{EDR_G}$ during summer months with the occurrence of smaller values of SZA and air masses. Values of r^2 varied from a maximum of 0.997 to a minimum of 0.917 with average of 0.98 ± 0.01 (1σ), while values of SD% varied correspondingly from a minimum of 1.5% to a maximum of 8.2% with an average of 3.4% ± 1.1%. 95% of the linear fittings had values of $r^2 \geq 0.95$ (very high) and SD% < 6%.

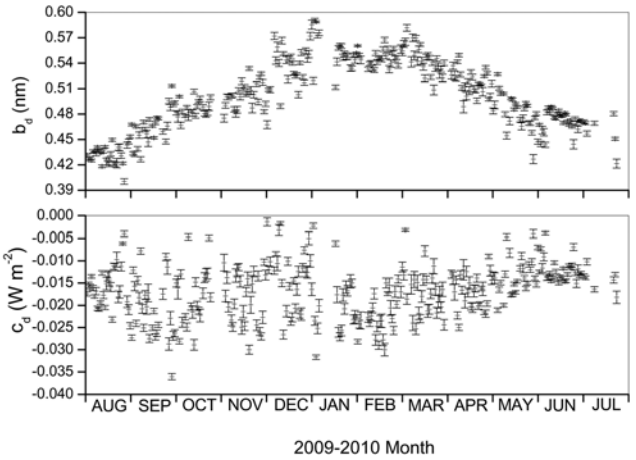

Fig. 4 The linear fitting parameters (top) b_d and (bottom) c_d from 293 linear fittings of S_G *vs.* $\mathrm{EDR_G}$ in BH. Uncertainties are 1σ.

The bottom frame of Fig. 5 shows the linear fitting for JAN022010, while Table 2 shows the fitting line parameters for this day and for DEC092009 and OCT162009. As a clear-sky and, practically, cloudless day, JAN022010 produces a fitting line with one of the highest r^2 and lowest SD% in this study. In addition, parameters c_d and b_d were significant at 95%. However, some weakness in this linear approach is found for the data inside the dashed-flat circle in the bottom frame of Fig. 5. These data correspond to the larger values of SZA in

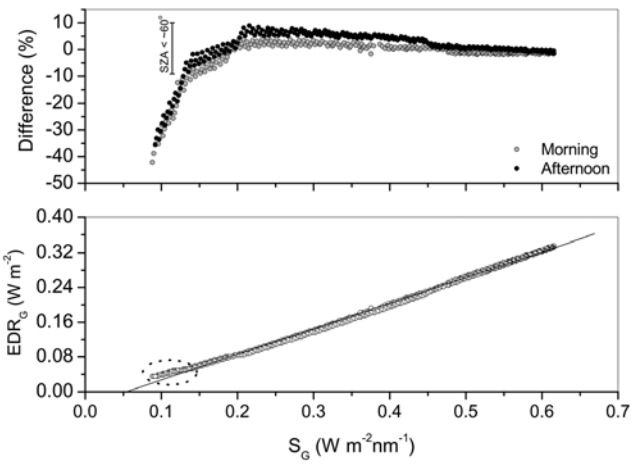

Fig. 5 Linear regression analysis applied to S_G *vs.* $\mathrm{EDR_G}$ on JAN022010 in BH. (Top) Percentage differences between the fitting line and measured values of $\mathrm{EDR_G}$. (Bottom) The fitting line between S_G and $\mathrm{EDR_G}$.

Table 2 Parameters from the linear fitting of S_G *vs.* EDR_G on JAN022010, DEC092009, and OCT162009 in BH. In the case, $EDR_G = c_d + b_d \cdot S_G$ with the coefficient of determination (r^2), the percent scattering of points (SD%) around the fitting line, and the number (N) of pairs of data. Uncertainties are 1σ

Day	c_d (W m^{-2})	b_d (nm)	r^2	SD (%)	N
JAN022010	−0.0317 ± 0.0005	0.589 ± 0.001	0.997	1.7	578
DEC092009	−0.0018 ± 0.0004	0.489 ± 0.003	0.989	2.8	358
OCT162009	−0.022 ± 0.001	0.498 ± 0.003	0.978	4.4	477

early morning and late afternoon. In this case, the UVA contribution to EDR_G is improved in relation to the UVB one. Since S_G includes no UVA wavelengths, the linear relation between S_G and EDR_G is weakened. The top frame of Fig. 5 shows the percentage differences between the fitting line and EDR_G. For SZA $\lessapprox 60°$, which are richer in UVB, the differences are inside the limits of ±10%, which are similar to the uncertainties in both S_G and EDR_G. Differences higher than ≈10% (<−10%) refer to data inside the dashed-flat circle.

The presence of clouds, especially those blocking the Sun, represents another scenario with capability to weaken the linear relation between S_G and EDR_G. The left-sided frames of Fig. 3 show the daily distributions of EDR_G measurements and their corresponding calculated values of EDR_{Dif} for JAN022010, DEC092009, and OCT162009, while Table 3 shows the daily average values of cloud cover for those days. JAN022010 depicts a distribution of solar radiation incidence regularly increasing towards noon, as expected for a cloudless day to which cloud cover was below 3%. The two other days depict a distribution of values strongly affected by cloud cover, which had daily average values of 70% and 100%. The presence of clouds changes the relative contribution of UVA and UVB to EDR_G. As S_G includes only UVB wavelengths, the linear relation between S_G and EDR_G becomes poorer. This is clearly indicated in Table 2 by the fitting line parameters for the two of the cloudy days. In the case, r^2 decreased, SD% increased, and b_c and c_d had higher uncertainties in comparison with JAN022010. The dependence of EDR_{Dif} on cloud cover will be discussed later.

Despite the occurrence of highly variable sky conditions typically regarding a tropical, urban site for 12 months, the linear fitting parameters of b_c and c_d obtained with 95% of confidence, $r^2 \geq 0.91$, and SD% < 6% for 95% of the fittings indicate the feasibility of the hypothesis of a linear relation between S_G and EDR_G.

Table 3 Parameter ρ, the daily average cloud cover represented by LCC_{60}, and the percentage (T%) of the elapsed time for measurements of S_G and EDR_G resulting in values of valid EDR_{Dif}

Day	ρ	Ave. LCC_{60} (%)	T (%)
JAN022010	0.093	2	90
DEC092009	0.090	100	50
OCT162009	0.102	70	73

Selecting values of valid EDR_{Dif}

The main drawback of situations leading to poorer linear fittings between S_G and EDR_G is the calculation of poorer quality EDR_{Dif} values. To identify and remove such values keeping only values of valid EDR_{Dif}, it is necessary to apply the filter represented by eqn (16). The amount of values of valid EDR_{Dif} will in general be shorter than the amount of values from a daily distribution of measurements of S_G and EDR_G. For instance, the dashed-horizontal line just above the time axis in the top-right frame of Fig. 3 shows the interval corresponding to valid EDR_{Dif} on JAN022010. This period of time is represented by the parameter T% defined as the percentage of time corresponding to the measurements of S_G and EDR_G leading to valid EDR_{Dif}. In Table 3, T% for DEC092009 is 50%. It means that only 50% of the values of EDR_{Dif} shown in the middle-left frame of Fig. 3 correspond to valid EDR_{Dif}. The elapsed time for measurements of S_G and EDR_G and the time corresponding to values of valid EDR_{Dif} had averages of 8 ± 1 h and 6 ± 1 h respectively. The application of the filter represented by eqn (16) to 293 daily distributions of EDR_G and their corresponding values of both EDR_{Dif} and $\bar{f}_4$ resulted in values of σ_ρ (eqn (15)) ranging from 0.091 to 0.104 with average of 0.094. It means there is an average uncertainty of 9.4% in the criterion for the selection of valid EDR_{Dif}.

Although every linear fitting in this study yielded $r^2 \geq 0.917$, there are many pairs of data in the database of S_G and EDR_G veering off in more than 10% the fitting line. They all showed some level of linear unbalance between S_G and EDR_G probably caused by changes in the relative contributions of UVA and UVB to the measurements. Checking on the TSI images corresponding to these cases reveals that the presence of clouds like Cumulus (Cu) and Cumulunimbus (Cb) blocking the Sun are linked with such linear unbalance.

Once the values of valid EDR_{Dif} have been identified, their final daily distributions are built. Such distributions are similar to the ones seen in the left-sided frames of Fig. 3, but they are composed of a lower number of data, which are proportional to T%.

The top frame of Fig. 6 depicts the daily maximum values of both EDR_G and valid EDR_{Dif}. They have not necessarily occurred at the same time for a given day. No value of valid EDR_{Dif} is found in the low range of UVI, and most of them were above the moderate range in the high and very high ranges of UVI. There were a few values in the extreme range mainly in the spring–summer months, which can be associated with events of radiation enhancement.[35] Utrillas *et al.*[36] have found UVI = 6 (high range) for Dif radiation at a Spanish town (39.51°N, 0.42°W, 30 m a.s.l.) close to the Mediterranean sea. Therefore, Dif radiation is obviously a dangerous component in solar UVR not only in terms of sunburn for lighter skin (types I and II), but also in relation to other damages potentially coming out for all skin types under chronic exposure.

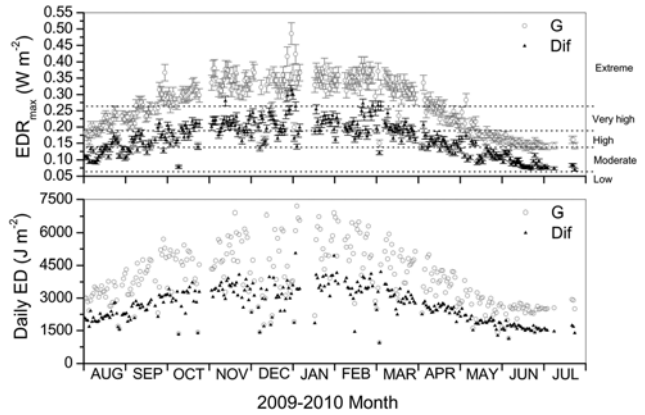

Fig. 6 (Top) Maximum daily values of both EDR_G and valid EDR_{Dif} in BH with uncertainties of 1σ. Ranges of UV-Index (UVI) are depicted on the right side of the frame: low UVI, EDR < 0.0625 W m^{-2}; moderate UVI, 0.0625 W m^{-2} ≤ EDR < 0.1375 W m^{-2}; high UVI, 0.1375 W m^{-2} ≤ EDR < 0.1875 W m^{-2}; very high UVI, 0.1875 W m^{-2} ≤ EDR < 0.2625 W m^{-2}; and extreme UVI, EDR ≥ 0.2625 W m^{-2}. (Bottom) Daily values of ED_G and ED_{Dif}, where 100 J m^{-2} of ED = 1 Standard Erythema Dose (SED).

The time integration of both valid EDR_{Dif} and its corresponding value of EDR_G for a period of time t proportional to T%,

$$ED_{Dif} = \int_0^t \text{valid}\, EDR_{Dif} \cdot dt \quad \text{and} \quad ED_G = \int_0^t EDR_G \cdot dt, \qquad (17)$$

respectively, lead to the diffuse erythemal dose (ED_{Dif}) and the global erythemal dose (ED_G). The ratio between them,

$$Dif/G = \frac{ED_{Dif}}{ED_G}, \qquad (18)$$

can be used in the extrapolation of a value for the daily incidence of ED_{Dif} (daily ED_{Dif}), taking the daily incidence of ED_G (daily ED_G) measured by BSL as reference. Thus,

$$\text{daily } ED_{Dif} = Dif/G \cdot \text{daily } ED_G. \qquad (19)$$

Daily ED_{Dif} is the value that would be obtained if all values of EDR_{Dif} were valid ones (T% = 100%). However, aspects like the lack of contribution of UVA wavelengths to S_G increase the uncertainty in daily ED_{Dif}, and the difference between this value and a real one decreases with T%. Hence, based on the values of T% presented in Table 3, the daily EDR_{Dif} for JAN022010 is of better quality than the value for OCT162009, and the latter is of better quality than the value for DEC092009. The bottom frame of Fig. 6 depicts both daily ED_G and daily ED_{Dif} in this study. The latter has an average of 2673 ± 788 J m^{-2} ranging from 936 J m^{-2} to 5053 J m^{-2}. The lowest value occurred for an overcast rainy day of fall (March 3 of 2010, Dif/G = 0.992, T% = 30%) where Cu clouds predominated in the sky, while the highest value corresponded to a summer day (January 1 of 2010, Dif/G = 0.83, T% = 77%) to which the daily average cloud cover was 86%. Cloud cover in this day varied from overcast skies of Cu in the morning to mid cloudy in the afternoon. However, the afternoon had Cu, Altostratus (As), and Altocumulus (Ac) spread in the sky. In addition to being thinner than typical Cu clouds, As and Ac also contribute significantly to events of solar radiation enhancement.[35] Note that, not only the daily ED_{Dif} value of 5053 J m^{-2} corresponds to 70% of the daily ED_G for the clear-sky and practically cloudless summer day of JAN022010, but also a value of EDR_{max} = 0.263 W m^{-2} in the range of extreme UVI was obtained for Dif radiation on that day.

The dependence of Dif/G on cloud cover

Clouds are important atmospheric agents of attenuation and scattering of solar radiation. Therefore, it seems natural to think of a connection between UV_{Dif} and clouds. Fig. 7 shows the analytic interpretation of the dependence of Dif/G on cloud cover represented by the daily average LCC_{60} parameter. It is a quadratic relation increasing form cloudless to overcast skies with good r^2 of 0.79 and medium SD% of 12%. Grant and Gao[37] have found a similar relation between Dif radiation and cloud cover. The SD% of 12% reflects part of the effect of clouds blocking the Sun. Size, shape, and constituents (water vapor, ice crystals, and hailstone) of clouds are likely to play an important role in this case. However, points around the quadratic curve are distributed uniformly. It suggests an effect of dispersion on the Dif/G ratio with roughly no dependence on cloud cover or other parameters in the study. For instance, cloudless skies had minimum Dif/G = 0.48, T% = 90%, TOC = 257.8 DU, and noon SZA = 4.5° on JAN022010, average Dif/G = 0.60, T% = 90%, TOC = 248.1 DU, and noon SZA = 43.4° on June 19 of 2010, and maximum Dif/G = 0.70, T% = 87%, TOC = 244.5 DU, and noon SZA = 43.2° on June 12 of 2010.

Aerosols had probably a significant influence on the data and perhaps they can explain partially the results. A clear influence of the turbidity caused by aerosols on Dif radiation has been found by Utrillas *et al.*[36] and McCartney,[38] where the relative contribution of UV_{Dif} to UV_G increases with turbidity. Con-

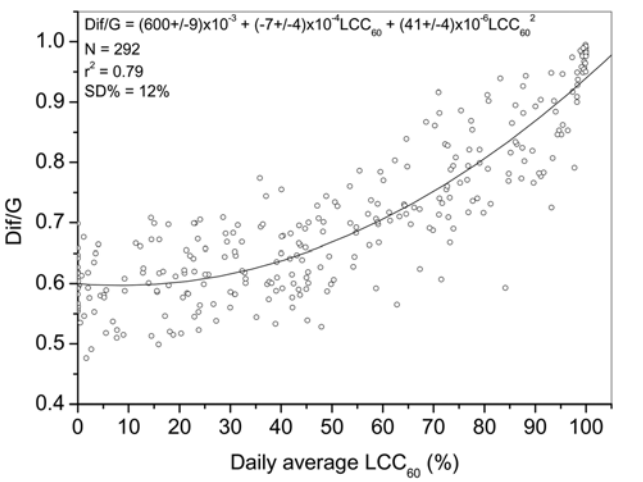

Fig. 7 The quadratic dependence of Dif/G on the cloud cover (LCC_{60}) in BH. Uncertainties are 1σ.

sidering just cloudless days of aerosol-free atmospheres simulated by the FastRT model, the difference between calculated values of EDR_G and UV_G and corresponding measurements by BSL and UVMFR4, respectively, makes an average value of UVR attenuation by aerosols of 15% ± 7%. This is a reasonable value similar to the ones found in other studies.[39,40] Trabelsi *et al.*[40] have found averages of 9% ± 6% for the attenuation of solar UVR by aerosols in cloudless days of a semi-arid Tunisian island (34.73°N, 11.30°W, 13 m a.s.l.). In the case, aerosols were a mix of crustal, sea salt, and anthropogenic sulfates. The standard deviations of 7% and 6% indicate the variability in the attenuation of UVR by aerosols, while the SD% of 12% indicates the additional contribution from clouds to that variability. Nevertheless, no net information is available for the time being regarding the effect of aerosols on Dif/*G* in BH, especially because the apportionment between local aerosols of absorption and scattering of UVR is still unknown.

Conclusions

The incidence of erythemal Dif radiation in a tropical, urban site was investigated for 12 months through a proposed method based on measurements of EDR_G, UV_G, and UV_{Dif}. The results are a quantitative source of reference on Dif radiation for a wide range of latitudes, as the SZA in the site ranged from 0° to 90°. Since UVMFR4 is not equipped with sensors for UVA wavelengths, the use of an instrument with additional channels in the UVA would improve the poorer linear relation between S_G and EDR_G caused by larger SZA and thick cumuliform clouds blocking the Sun.

The dependence on clouds was investigated analytically. The Dif/*G* ratio increased as a quadratic function of cloud cover. A minimum of 0.48 was found for a practically cloudless sky, while an average of 0.6 and a maximum of 0.70 were found for cloudless skies too. Clouds are the most powerful atmospheric constituent influencing the incidence of UVR. In general, while clouds blocking the Sun reduce the incidence of Dir radiation, the thinner As and Ac can promote radiation enhancement through Dif radiation.

Except for the typical average attenuation of 15% of UVR by aerosols, no other influence of aerosols on Dif radiation has been determined. The matter merits further investigation.

Most of the maximum values of valid EDR_{Dif} reached the high and very high ranges of UVI, and some of them reached even the extreme range in the spring–summer period. No value was found in the low range. In terms of daily ED_{Dif}, values with average of 2673 J m^{-2} ranging from 936 J m^{-2} (overcast skies of Cu in fall) to 5053 J m^{-2} (cloudy summer day with cloud cover of 86% by Cu, As, and Ac predominantly) were found. Dif radiation represents a real threat in terms of acute effects like sunburn for skin types I and II, or long term effects from chronic exposures for every skin type. Its incidence must be seriously considered in the tropics.

Annex A – List of acronyms

BH	Belo Horizonte
BSL	Biometer Solar Light 501A
CIE	Commission Internationale de l'Éclairage
Dif	Diffuse component of radiation
Dir	Direct component of radiation
DISORT	Discrete ordinates radiative transfer equation solver
DU	Dobson units
ED_{Dif}	Diffuse erythemal dose
ED_G	Global erythemal dose
EDR_{Dif}	Diffuse erythemal dose rate
EDR_G	Global erythemal dose rate
FastRT	Fast and easy simulation tool for radiation transfer calculation
G	Global radiation
JPEG	Joint Photographic Experts Group
LCC_{60}	Local cloud cover over 60 minutes
LLUV	Laboratório de Luz Ultravioleta
S_{Dif}	Sum of the diffuse ultraviolet radiation rate values
S_G	Sum of the global ultraviolet radiation rate values
SZA	Solar zenith angle
TOC	Total ozone column
TSI	Total Sky Imager 440A
UT	Universal time
T%	Percentage of time corresponding to the measurements of S_G and EDR_G leading to valid EDR_{Dif}
UV_{Dif}	Diffuse ultraviolet radiation rate
UV_{Dir}	Direct ultraviolet radiation rate
UV_G	Global ultraviolet radiation rate
UVA	Ultraviolet radiation in the range of 320–380 nm
UVB	Ultraviolet radiation in the range of 280–320 nm
UVI	UV-Index
UVMFR4	Ultraviolet Rotating Shadowband Radiometer 4
UVR	Ultraviolet radiation
VD	Vitamin D

Acknowledgements

This study was financially supported by Conselho Nacional de Desenvolvimento Científico e Tecnológico (CNPq, grant 471159/2004-2 and other grants), Fundação de Amparo à Pesquisa do Estado de Minas Gerais (FAPEMIG, CRA 25/03 and CRA APQ 0848-5.02/07), and logistic supported by PUC Minas.

References

1 WHO, *Ultraviolet radiation, EHC 160*, World Health Organization, Geneva, Switzerland, 1994.
2 P. Kullavanijaya and H. W. Lim, Photoprotection, *J. Am. Acad. Dermatol.*, 2005, **52**, 937–958.
3 S. Lautenschlager, H. Christian Wulf and M. R. Pittelkow, Photoprotection, *Lancet*, 2007, **370**, 528–537.

4 T. B. Fitzpatrick, The validity and practicality of sunreactive skin types I through VI, *Arch. Dermatol.*, 1988, **124**, 869–871.

5 WHO, *Global solar UV Index: a practical guide*, World Health Organization, Geneva, Switzerland, 2002.

6 K. P. Nielsen, L. Zhao, J. J. Stamnes, K. Stamnes and J. Moan, The importance of the depth distribution of melanin in skin for DNA protection and other photobiological processes, *J. Photochem. Photobiol., B*, 2006, **82**, 194–198.

7 J. Moan, A. Dahlback and R. B. Setlow, Epidemiological support for a hypothesis for melanoma induction indicating a role for UVA radiation, *Photochem. Photobiol.*, 1999, **70**, 243–247.

8 M. F. Holick, Vitamin D deficiency, *N. Engl. J. Med.*, 2007, **357**, 266281.

9 B. A. Ingraham, B. Bragdon and A. Nohe, Molecular basis of the potential of vitamin D to prevent cancer, *Curr. Med. Res. Opin.*, 2008, **24**, 139–149.

10 M. Berwick and D. Kesler, Ultraviolet radiation exposure, vitamin D, and cancer, *Photochem. Photobiol.*, 2005, **81**, 1261–1266.

11 M. Norval, L. O. Björn and F. R. de Gruijl, Is the action for the UV-induced production of previtamin D_3 in human skin correct?, *Photochem. Photobiol. Sci.*, 2010, **9**, 11–17.

12 M. Kimlin, S. Harrison, M. Nowak, M. Moore, A. Brodie and C. Lang, Does a high UV environment ensure adequate vitamin D status?, *J. Photochem. Photobiol., B*, 2007, **89**, 139–147.

13 N. Binkley, R. Novotny, D. Krueger, T. Kawahara, Y. G. Daida, G. Lensmeyer, B. W. Hollis and M. K. Drezner, Low vitamin D status despite abundant sun exposure, *J. Clin. Endocrinol. Metab.*, 2007, **92**, 2130–2135.

14 B. Lehmann, The vitamin D_3 pathway in human skin and its role for regulation of biological processes, *Photochem. Photobiol.*, 2005, **81**, 1246–1251.

15 M. F. Hollick, Sunlight and vitamin D for bone health and prevention of autoimmune diseases, cancers, and cardiovascular disease, *Am. J. Clin. Nutr.*, 2004, **80**, 1678S–1688S.

16 A. A. Silva, Improving photoprotection attitudes in the tropics: sunburn vs vitamin D, *Photochem. Photobiol.*, 2014, **90**, 1446–1454.

17 C. Gordon-Thomson, R. Gupta, W. Tongkao-on, A. Ryan, G. M. Halliday and R. S. Mason, 1α,25 dihydroxyvitamin D_3 enhances cellular defenses against UV-induced oxidative and other forms of DNA damage in skin, *Photochem. Photobiol. Sci.*, 2012, **11**, 1837–1847.

18 D. D. Bikle, Protective actions of vitamin D in UVB induced skin cancer, *Photochem. Photobiol. Sci.*, 2012, **11**, 1808–1816.

19 CIE, *Recommendations on minimum levels of solar UV exposure, CIE 201:2011*, Commission Internationale de L'Eclairage, 2011.

20 R. M. Sayre and J. C. Dowdy, Darkness at noon: sunscreens and vitamin D_3, *Photochem. Photobiol.*, 2007, **83**, 459–463.

21 J. Reichrath, The challenge resulting from positive and negative effects of sunlight: How much solar UV exposure is appropriate to balance between risks of vitamin D deficiency and skin cancer?, *Prog. Biophys. Mol. Biol.*, 2006, **92**, 9–16.

22 B. Diffey, Do we need a revised public health policy on sun exposure?, *Br. J. Dermatol.*, 2006, **154**, 1046–1051.

23 D. Wolpowitz and B. A. Gilchrest, The vitamin D questions: How much do you need and how should you get it?, *J. Am. Acad. Dermatol.*, 2006, **54**, 301–317.

24 A. R. Young and S. L. Walker, UV radiation, vitramin D and human health: an unfolding controversy introduction, *Photochem. Photobiol.*, 2005, **81**, 1243–1245.

25 A. V. Parisi and D. J. Turnbull, Shade provision for UV minimization: a review, *Photochem. Photobiol.*, 2014, **90**, 479–490.

26 B. Diffey, Sunscreen isn't enough, *J. Photochem. Photobiol., B*, 2001, **64**, 105–108.

27 L. R. Sklar, F. Almutawa, H. W. Lim and I. Hamzavi, Effects of ultraviolet radiation, visible light, and infrared radiation on erythema and pigmentation: a review, *Photochem. Photobiol. Sci.*, 2013, **12**, 54–64.

28 A. F. Bais, R. L. McKenzie, G. Bernhard, P. J. Aucamp, M. Ilyas, S. Madronich and K. Tourpali, Ozone depletion and climate change: impacts on UV radiation, *Photochem. Photobiol. Sci.*, 2015, **14**, 19–52.

29 CIE, *Erythema reference action spectrum and* standard erythemal dose, CIE S 007/E-1998, Commission Internationale de l'Eclairage, Vienna, Austria, 2000.

30 G. Hulsen and J. Gröbner, Characterization and calibration of ultraviolet broadband radiometers measuring erythemally weighted irradiance, *Appl. Opt.*, 2007, **46**, 5877–5886.

31 G. Bernhard and G. Seckmeyer, Uncertainty of measurements of spectral solar UV irradiance, *J. Geophys. Res.*, 1999, **104**, 14321–14345.

32 A. A. Silva and M. P. Souza-Echer, Ground-based measurements of local cloud cover, *Meteorol. Atmos. Phys.*, 2013, **120**, 201–212.

33 O. Engelsen and A. Kylling, Fast simulation tool for ultraviolet radiation at the Earth's surface, *Opt. Eng.*, 2005, **44**, 041012.

34 A. A. Silva and L. M. Tomaz, Total ozone column measurements for an urban, tropical site in the Southern Hemisphere with a Microtops II, *J. Atmos. S-Terr. Phys.*, 2012, **77**, 161–166.

35 A. A. Silva, Erythemal dose rate under noon overcast skies, *Photochem. Photobiol. Sci.*, 2013, **12**, 777–786.

36 M. P. Utrillas, M. J. Marín, A. R. Esteve, F. Tena, J. Cañada, V. Estellés and J. A. Martínez-Lozano, Diffuse UV erythemal radiation experimental values, *J. Geophys. Res.*, 2007, **112**, D24207, DOI: 10.1029/2007JD008846.

37 R. H. Grant and W. Gao, Diffuse fraction of UV radiation under partly cloudy skies as defined by the Automated

Surface Observation System (ASOS), *J. Geophys. Res.*, 2003, **108**, 4046, DOI: 10.1029/2002JD002201.

38 H. A. McCartney, Spectral distribution of solar radiation. II: global and diffuse, *Quart. J. Roy. Met. Soc.*, 1978, **104**, 911–926.

39 A. A. Silva, Local cloud cover, ground-based and satellite measurements of erythemal dose rate for an urban, tropical site in Southern Hemisphere, *J. Atmos. S- Terr. Phys.*, 2011, **73**, 2474–2481.

40 A. Trabelsi, M. Saad, M. Masmoudi and S. C. Alfaro, Atmospheric aerosols and their impacto n surface solar irradiation in Kerkennah Islands (eastern Tunisia), *Atmos. Res.*, 2015, 102–107.